

# In situ analysis of the fragmentation of polystyrene films within sliding contacts

A. Chateauminois<sup>a,\*</sup>, M.C. Baietto-Dubourg<sup>b</sup>, C. Gauthier<sup>c</sup>, R. Schirrer<sup>a</sup>

<sup>a</sup>Laboratoire de Physico-Chimie des Polymères et des Milieux Dispersés, UMR 7615, Ecole Supérieure de Physique et de Chimie Industrielles (ESPCI), 10 rue Vauquelin, 75231 Paris, Cedex 05, France

<sup>b</sup>Laboratoire de Mécanique des Contacts et du Solide, UMR 5514, INSA de Lyon, 18-20, rue des Sciences, F69621 Villeurbanne Cedex, France

<sup>c</sup>Institut Charles Sadron, UPR 22, 6, rue Boussingault, F-67083 Strasbourg, France

Available online 25 August 2005

## Abstract

Fracture processes of thin (10–100  $\mu\text{m}$ ) polystyrene films on PMMA substrates have been investigated within macroscopic single-asperity sliding contacts with rigid spheres. Using the resources of in situ contact visualization, the development of cracks has been analyzed under both elastic and plastic conditions for various values of the ratio of the contact radius to the film thickness. Under elastic contact conditions, damage mechanisms were dominated by the formation of a network of regularly spaced cracks at the leading edge of the contact. These processes were analyzed in the light of a fragmentation model based on contact mechanics simulations of the stress field induced within the cracked films. It emerged from this contact mechanics analysis that the mean spacing between adjacent cracks can be correlated to the strength of the polymer coating.

© 2005 Elsevier Ltd. All rights reserved.

**Keywords:** Polystyrene films; Fracture; Sliding; Scratch; Fragmentation

## 1. Introduction

Polymeric coatings are largely used to improve contact mechanical and tribological performance of engineering materials and optical components. However, the development and selection of such films is a very complex and costly task. The number of parameters is huge, spanning from material, physical, mechanical and surface properties to the behaviour of complex films/substrate systems. In addition, there is a lack of data and understanding regarding the actual deformation and fracture mechanisms involved in such coatings.

Within this context, abrasion resistance remains one of the key issues regarding the lifetime of organic coatings. During abrasive wear damage, the initial stage is usually considered to be the process of contact and scratch between the polymer surface and a sharp asperity. The accumulation of the associated microscopic failure events eventually generates wear particles and gives rise to weight loss.

Investigating such processes within macroscopic contacts between rough surfaces is, however, a difficult task due to the multiple interactions between individual sliding micro-asperities. In order to overcome these limitations, model experiments are often considered which attempt to simulate the damage induced by a single asperity contact [1]. Although the wear rate itself is not monitored, such experiments provide the opportunity of getting a more detailed insight into the deformation and fracture mechanisms involved in asperity engagements. In such experiments, the selection of different indenter geometries and loading conditions offers the possibility of exploring the viscoelastic/viscoplastic response and brittle failure mechanisms over a wide range of strains and strain rates. For bulk polymers, the observed damage evolves through a range of severity as the contact strain is increased: visco-elastic smoothing or ‘ironing’, plastic or viscoplastic grooving, extensive plastic flow and tearing, pronounced fracture or tearing and finally cutting or chip formation can be identified [2–8]. These approaches have been popularized for a variety of amorphous and glassy and semi-crystalline polymers by Briscoe and co-workers [9,10] who put together in the form of ‘deformation maps’ the different deformation regimes.

\* Corresponding author. Tel.: +33 1 40 79 47 87; fax: +33 1 40 79 46 86.

E-mail address: antoine.chateauminois@espci.fr (A. Chateauminois).

### Nomenclature

$a$	radius of the contact area	$L_c^{\text{th}}$	theoretical critical length between two adjacent cracks under sliding conditions
$h$	film thickness	$\delta$	relative displacement between the leading edge of the contact and the location of a crack
$K_I$	Mode I crack tip stress intensity factor	$\mu$	coefficient of friction
$P$	applied normal load	$\sigma_{xx}^{\text{max}}$	Maximum value of the surface tensile stress
$p_0$	maximum Hertzian contact pressure		
$R$	radius of the sphere counterface		
$L_c^{\text{exp}}$	experimental critical length between two adjacent cracks under sliding conditions		

Similar regimes can be identified in the case of polymeric coatings. Within the fracture domain, regular crack patterns are often observed at the leading edge of the contact under the action of predominantly tensile stresses [7,8,11,12]. A critical normal force is often ascribed to the occurrence of such cracking processes, but the way it relates to known polymer failure properties such as fracture toughness is still a matter of debate [6]. In addition, the contribution of substrate deformation to the development of contact cracks within thin polymer films remains largely unknown. As a first approach, the magnitude of these effects may be assumed to depend largely on the ratio of the contact area,  $a$ , to the film thickness,  $h$ . In many contact situations, this  $a/h$  ratio can vary by orders of magnitude depending on whether the macroscopic or micro-asperity contact lengths are considered. There is therefore a need for a better understanding of coating fracture processes as a function of this characteristic  $a/h$  ratio.

Within the frame of this investigation, fracture mechanisms of thin (10–100  $\mu\text{m}$ ) polystyrene (PS) films on polymethacrylate (PMMA) substrates have been investigated within macroscopic sliding contacts with smooth spherical asperities. Using the resources of in situ contact visualization, the various stages of the development of crack networks within the PS film have been observed for a range of contact conditions which were characterized by different ratios of the contact radius,  $a$ , to the film thickness,  $h$ . The resulting crack patterns have been analyzed in the light of a fragmentation model which considers that failure is driven by the evolving tensile stress field induced within the cracked PS film at the leading edge of the contact. For that purpose, a contact mechanics analysis of the cracked coated systems has been developed which is able to simulate the film unloading/reloading processes associated with the propagation of successive cracks during sliding.

## 2. Experimental details

### 2.1. Elaboration of the film systems

The polymer systems investigated in this study consisted in a poly(methylmethacrylate) (PMMA) substrate coated

with poly(styrene) (PS) films 10–100  $\mu\text{m}$  in thickness. In order to promote an optimum stress transfer between the two polymer layers, a thin (about 40 nm) layer of a PS-b-PMMA block copolymer was inserted at the PS/PMMA interface during the processing of the specimens. Mode I fracture tests carried out by Brown et al. [13] indicated that such di-block polymers can dramatically improve the adhesion between PS and PMMA, provided that the thickness of the copolymer layer is greater than one fourth of the polymer long period, which was the case in the present study.

Both the PMMA and PS polymers were provided as pellets by Atofina (France). Their molecular and mechanical properties are given in Table 1. The PS-b-PMMA block copolymer was provided by Polymer Source Inc. (Canada). The number average molecular weights of the PS and PMMA arms were  $8 \times 10^4$  and  $9.1 \times 10^4 \text{ g mol}^{-1}$ , respectively.

The PMMA substrate was obtained by compression moulding of pellets at 160  $^\circ\text{C}$  between two thick float glass plates which allowed minimizing the surface roughness. All the plates were 6 mm thick.

The block copolymer was directly spun-cast on the PMMA plates from a 0.8 w% solution in toluene. Separate measurements by ellipsometry using silicon wafers as a substrate indicated that, for the selected spin coating conditions, the thickness of the copolymer layer was about 40 nm.

The polystyrene films were elaborated independently by dip coating on float glass plates. Pyrolyzed (600  $^\circ\text{C}$ ) glass plates were removed at constant speed from a 10% wt solution of PS in toluene at R.T. A preliminary investigation

Table 1  
Mechanical properties of the polymers (from ref [35])

	PMMA	PS
$M_w$ ( $10^3 \text{ g/mol}$ )	68	200
$T_g$ ( $^\circ\text{C}$ by DSC)	114	98
$E$ (GPa at 25 $^\circ\text{C}$ )	3.3	3
$\sigma_y$ (MPa)	136	105
$\sigma_c$ (MPa)	100	55
$\nu$	0.4	0.35

$E$  is the Young's modulus,  $\nu$  is the Poisson's ration.  $\sigma_y$  and  $\sigma_c$  denote the yield and the crazing stress, respectively.

showed that it was possible to vary the film thickness in the range 10–100  $\mu\text{m}$  by varying the removal speed of the plate and the number of dipping cycles. Profilometry measurements also showed that the thickness of the dip coated films did not vary by more than  $\pm 2 \mu\text{m}$  within the region used for the contact experiments.

In the final processing stage the PS coated glass plates were directly pressed in the heated press (160  $^{\circ}\text{C}$ , two hours) against the PMMA substrates covered with the copolymer layer. The specimens were subsequently allowed to cool down slowly at RT before demolding. Roughness measurements by interferometry indicated that the maximum peak-to-valley height,  $R_t$ , of the film surface was in the order of 30 nm.

## 2.2. Tribological tests

The film damage processes were investigated within sliding contacts with rigid spherical indenters. Using the resources of in situ contact visualization, the occurrence of contact cracks was investigated for various ratios of the contact radius,  $a$ , to the film thickness,  $h$  (Fig. 1). For that purpose, two separate experimental devices were used:

- (i) Low  $a/h$  ratios (in the order of the unity) were achieved by means of a specific scratching machine, the so-called ‘microvisioscratch’ device. This machine, which is fully described elsewhere [2], allows to scratch the surface of polymer materials using a rigid tip under imposed normal load and scratch velocity. During the tests, the velocity of the moving tip and the normal and tangential loads are continuously recorded. In addition, a built-in microscope allows in situ observation and measurement of the groove left on the surface. In the experiments to be detailed, the speed of the tip was kept constant to  $10 \mu\text{m s}^{-1}$  while the normal load was varied stepwise during each scratch test in as many steps as required to explore the desired strain range. The used tips were spherical diamond indenters having various radii of

curvature, namely 116 and 240  $\mu\text{m}$ . A steel ball with a 5 mm radius was also used. During the experiments, the average strain,  $a/R$ , varied from about 0.1 to 0.4 and the mean contact pressure from approximately 80–200 MPa, which corresponds to contact conditions ranging from elastic to plastic responses.

- (ii) The second tribological device allowed performing sliding tests under predominantly elastic conditions within macroscopic contacts about one millimetre in diameter, i.e. for  $a/h$  ratios ranging from about 10–100. It consisted in a specific reciprocating sliding device, which was used in the present investigation in a single-pass sliding mode. For a detailed description of this device, the reader is sent to reference [14]. Sphere-on-flat contacts under constant imposed normal force (between 10 and 250 N) were realized using plano-convex glass lenses of various radii of curvature (from 5.2 to 20.7 mm). During the experiments, a continuous tangential motion at constant velocity ( $10 \mu\text{m s}^{-1}$ ) was applied to the polymer specimen with respect to the fixed glass lens. Both the normal load and the tangential forces were continuously monitored. Simultaneously, a microscope and CCD camera coupled with an image acquisition device allowed to record contact pictures through the glass lens. Depending on the radius of the lens,  $R$ , and the normal load, the mean contact pressure ranged from about 40 to 120 MPa. The corresponding average strain,  $a/R$ , varied from 0.015 to 0.1.

## 2.3. Numerical simulations

Theoretical simulations were undertaken in order to assess the distribution of contact stresses within the cracked polystyrene film under elastic conditions. The approach was based on semi-analytical and semi-numerical contact mechanics algorithms which allow calculating stress fields and stress intensity factors at the cost of a moderate computational cost. Such calculations have already been successfully applied to the analysis of contact fatigue behaviour of epoxy materials [15]. Within the frame of this investigation, the coating fragmentation processes were analyzed using an equivalent two-dimensional, cylinder-on-cracked-flat configuration. For a given  $a/h$  ratio, the bidimensional contact conditions were adjusted in order to achieve the same maximum value of the tensile stress at the leading edge of the contact (where cracks were found to nucleate) than for the equivalent three dimensional sphere-on-flat configuration.

The used contact model rests on linear fracture mechanics and on an analogy between cracks and continuous distributions of dislocations. A distribution of cracks of given lengths, orientations and locations within the contact can be introduced in the model. Dubourg et al. [16] have developed a frictional contact crack model that allows taking into account the existence of multiple cracks within a contact field by

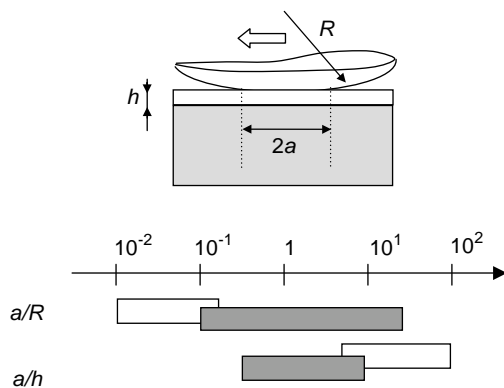


Fig. 1. Investigated ranges of mean contact strain,  $a/R$ , and ratio of the contact radius to film thickness,  $a/h$ , for the two different experimental setups used in this study. White boxes: reciprocating sliding tribometer; grey boxes: scratch tester.

modifying the pioneering formulation proposed by Cominou [17] and combining it with unilateral contact techniques. Interactions between cracks are automatically determined and accounted for, as well as the closure-opening-sliding sequences along the faces of the cracks during the loading cycle. Mode I and mode II effective stress intensity factors under non proportional multiaxial sequential loadings can also be calculated at crack tips.

Within the frame of this investigation, simulations were carried out assuming that the coating cracks were straight cracks oriented perpendicular with respect to the surface. Although it was not possible to support this hypothesis by

reliable direct observations of cross sections of the cracked PS films, previous investigations using brittle epoxy polymers under similar contact conditions [15] indicate that this is a reasonable approximation. Both observations and contact mechanics simulations showed that the cracks which nucleate at the edge of the contact (as observed for the PS coating, see below) propagate perpendicularly to the surface under a predominantly mode I tensile field. These conclusions were found to hold up to cracks depths which corresponded approximately to the contact radius. For the present numerical simulations, the maximum crack depth did not exceed one half of the contact radius.

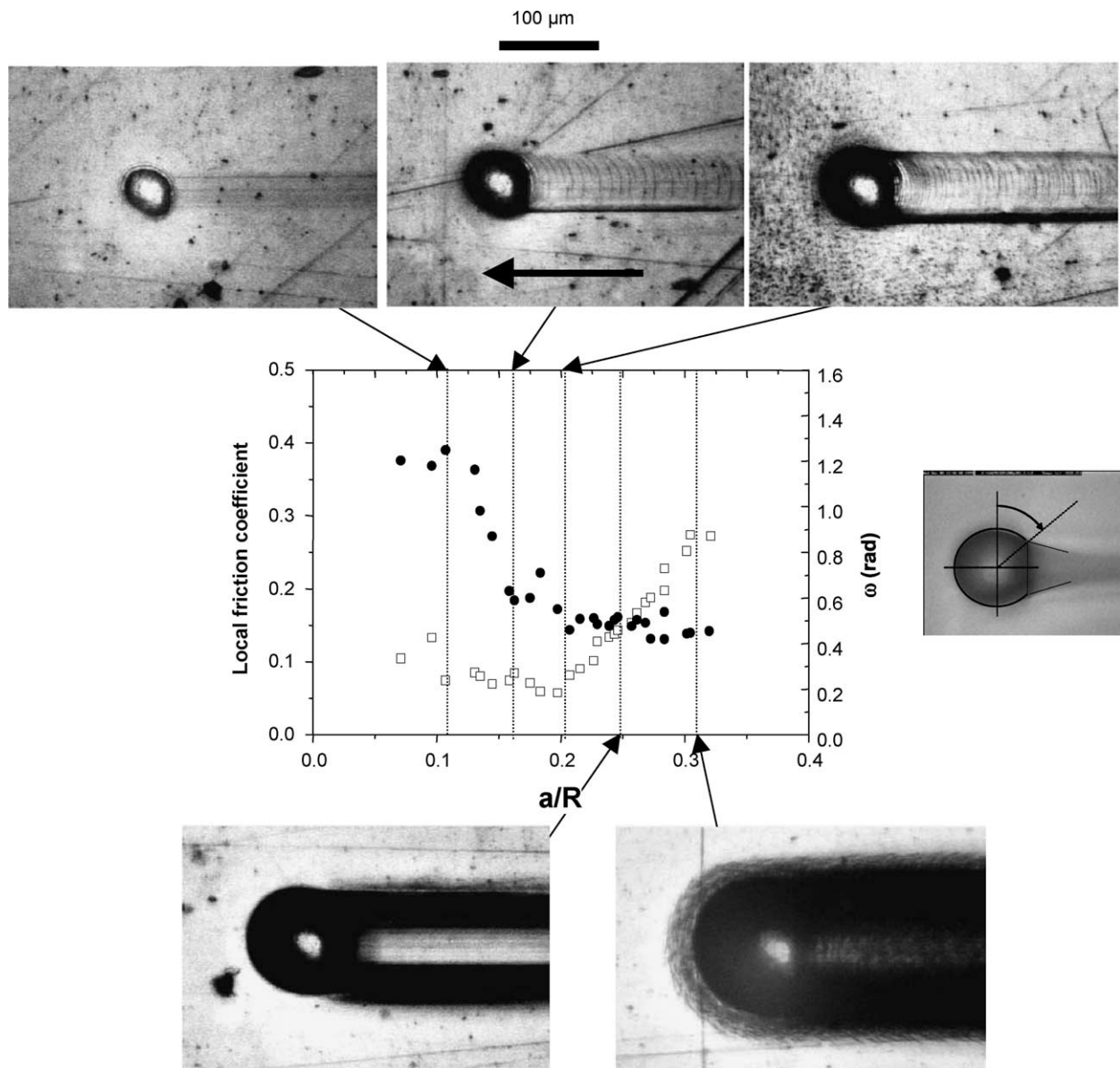


Fig. 2. Deformation modes and fracture processes within a contact between a 50  $\mu\text{m}$  coating and a spherical diamond tip with a 240  $\mu\text{m}$  radius of curvature. ( $\bullet$ ) contact rear angle,  $\omega$ ; ( $\square$ ) local friction coefficient, as calculated using the flow lines model detailed in references [27,28]. As the contact strain,  $a/R$ , increases, the transition from viscoelastic to plastic contact conditions is indicated by the increased contact dissymmetry, i.e. by a decrease in the contact rear angle,  $\omega$ . During this experiment the ratio of the contact radius to the film thickness ratio varied from 0.2 to 1.6.

### 3. Results

#### 3.1. In situ analysis of film cracking processes

The contact deformation behaviour and damage modes were at first investigated for moderate  $a/h$  ratios using the ‘microvisioscratch’ device. In order to vary the average contact strain,  $a/R$ , from elastic to plastic conditions, the normal load was incrementally increased during the lateral displacement of the tip. For each normal load step, in situ observations allowed to identify the nature of the contact loading from an analysis of the actual shape of the contact area. A typical example of the changes in the contact shape as a function of the average contact strain,  $a/R$ , is shown in Fig. 2 for a PS film 50  $\mu\text{m}$  in thickness and a 240  $\mu\text{m}$  radius tip. As detailed in references [2,3,18], the deformation response of the polymer surface can mainly be defined from a measurement of the contact rear angle,  $\omega$ , which is reported in the figure. At normal loads of a few tenths of a Newton, i.e.  $a/R$  ratios less than about 0.1, the tip slides elastically over the surface of the polymeric material and no residual groove is observed. The contact area is circular and the rear angle,  $\omega$  is therefore equal to  $\pi/2$ . The observed slight decrease in  $\omega$  when  $a/R$  ratios become close to 0.15 is indicative of the occurrence of viscoelastic effects: these processes induce the formation of a groove which relaxes within a time comparable to the contact time. Within this deformation regime, a network of curved cracks concave to the wake of the spherical indenter was observed. Such cracking processes present close similarities with the surface cracks which were observed under sliding spherical indenters by Bethune [12] for bulk polystyrene and by Sadeghipour et al. [19,20] and by Chateauinois et al. [21–23] for epoxy materials. They are also reminiscent of the so-called ‘partial Hertzian cones’ observed by Lawn and co-workers [24,25] when a sphere is translated across a glass surface under purely elastic conditions. According to Hamilton’s contact mechanics analysis [26], such cracks can be attributed to the predominantly tensile nature of the stress field at the leading edge of the contact.

When the contact strain,  $a/R$ , is further increased up to about 0.2, the transition from viscoelastic sliding to viscoplastic scratching conditions is indicated by a strong decrease in the contact rear angle and the formation of a permanent groove in the wake of the contact. This regime is characterized by a partial viscoelastic recovery of the groove, the material being predominantly subjected to plastic strains under the contact. This transition to viscoplastic conditions was associated with a disappearance of the curved cracks network.

As contact strain becomes greater than 0.25, some pile-up is observed in the front of the contact zone. Simultaneously, some cracking processes are detected in the frontal push-pad. As opposed to cracks induced under viscoelastic contact conditions, these cracks are convex to

wake of the contact. They result probably from the bending stresses associated with frontal pile-up.

A flow lines model detailed elsewhere [27,28] was also used to determine the value of the true (i.e. interfacial) coefficient of friction as a function the contact strain (Fig. 2). The occurrence of plastic deformation within the contact (for  $a/R > 0.2$ ) is associated with an increase in the interfacial friction while a nearly constant value of about 0.1 is achieved within the viscoelastic regime. These values of the local coefficient of friction were used to assess the magnitude of the tensile stresses at the leading edge of the contact using Hamilton and Goodman’s equations for the sliding of a rigid sphere on a semi-infinite elastic substrate. Although these expressions have been defined for elastic contact conditions, they were, to a first approximation, assumed to remain valid as long as the contact strain is lower than 0.2, i.e. as long as the contact is not completely plastic, which corresponds to the regime where cracks were initiated at the rear of the contact. In Fig. 3, the calculated maximum tensile stresses have been reported as a function of the mean contact strain, together with the values of the mean contact pressure. This later parameter was measured from the ratio of the normal load to the actual contact area. It increases with the contact strain up to a plateau value of about 200 MPa which corresponds to plastic contact conditions. For the PS coating under consideration, the calculated tensile stress in the viscoelastic cracking regime was about 50 MPa. An unexpected result is that this tensile stress remains constant while the mean contact pressure increases. This can be attributed to the fact that the true local friction coefficient decreases from 0.1 to 0.05 as the ratio  $a/R$  increases from 0.1 to 0.2. There is therefore some indication that the cracks induced at the rear edge of the viscoelastic contacts could regulate the friction level.

Using the modified reciprocating sliding device, additional tests have been carried out at large  $a/h$  ratios

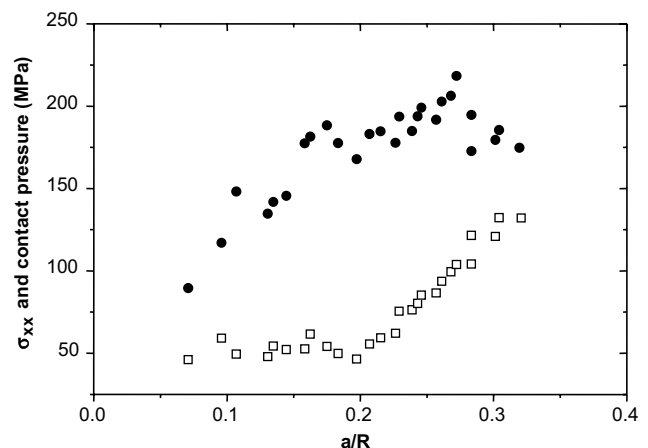


Fig. 3. Mean contact pressure (●) and maximum calculated tensile stress (□) at the rear edge of the contact as a function of the contact strain (50  $\mu\text{m}$  coating—240  $\mu\text{m}$  tip radius). The maximum tensile stress has been calculated from the true local coefficient of friction and the mean contact pressure using Hamilton’s theory [26].

( $ah > 10$ ) under predominantly elastic conditions. As it was observed in the viscoelastic regime for small  $ah$  ratios, the damage induced by the sliding motion consisted in the development of a network of curved cracks concave to the wake of the spherical indenter. No cracks were observed within uncoated PMMA substrate under similar contact conditions, which tends to indicate that cracks were localized within the PS coating. The enlarged size of the contacts allowed to capture the details of the development of the crack pattern from the resources of in situ contact visualization (Fig. 4). At the onset of the tangential loading, an initial crack is nucleated at the rear edge of the contact, where the surface tensile stress reaches its maximum value. Subsequent cracks are observed to

nucleate not exactly at the leading edge of the contact but at two symmetrical locations with respect to the contact meridian plane. As the sliding distance is further increased, regularly spaced cracks are simultaneously nucleated at the contact edge along two opposite locations which make an angle of about  $45^\circ$  with respect to an axis oriented along the sliding direction and passing through the centre of the contact. Once formed, these cracks tend to propagate slowly toward the rear of the contact along curvilinear paths. Cracks which nucleate at opposite locations with respect to the sliding direction eventually merge at the leading edge of the contact to give the final concave crack pattern left in the wake of the indenter after the removal of the glass slider.

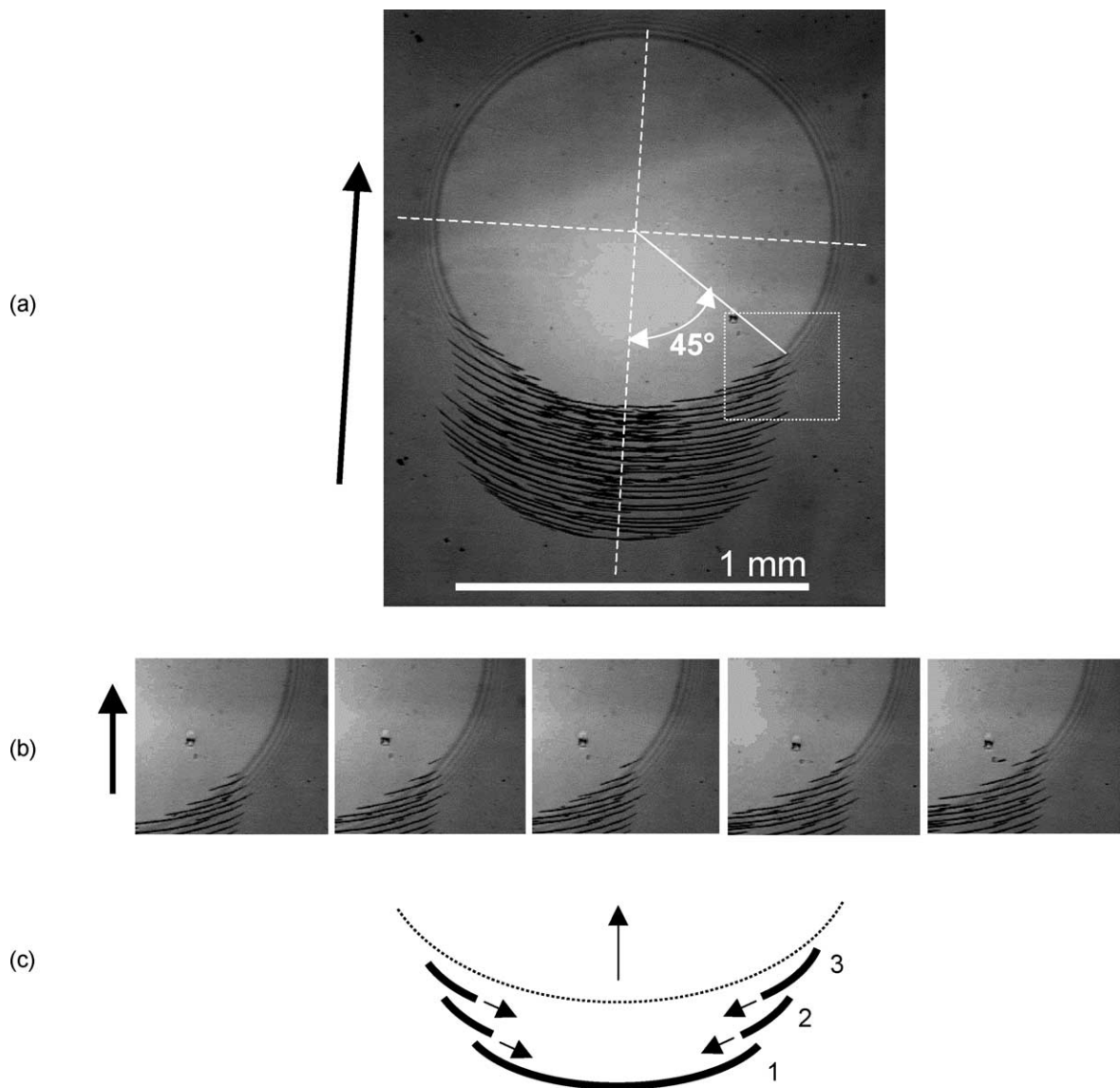


Fig. 4. In situ observation of the development of a crack pattern in the PS film under elastic sliding conditions. The contact strain is  $a/R=0.032$ , the ratio of the contact radius to the film thickness is 45. (a) Overall view of the contact during the sliding process. The insert box delimits the magnified area shown in Fig. b. (b) Details of the contact showing the successive nucleation of cracks and their propagation toward the rear of the contact. (c) Schematic description of the initial crack nucleation and propagation stages. Cracks 1, 2 and 3 are successively nucleated according to an unloading/reloading process associated to crack opening mechanisms and to the sliding of the rigid counterface.

A simple elastic contact mechanics analysis can provide some preliminary insight into the development of such a crack network. Due to the similarity of the PMMA and PS Young's moduli (cf Table 1), the coated polymer system can reasonably be assimilated to a homogeneous semi-infinite body. If the perturbations of the stress field due to the occurrence of cracks are neglected in a first approach, the tensile stresses at the edge of the contact can be estimated analytically using Hamilton's theory. Accordingly, the principal surface stresses,  $\sigma_1$  and  $\sigma_2$ , have been calculated along the curvilinear abscissa corresponding to the leading edge of the contact. As shown in Fig. 5, the coordinate along this curvilinear path was defined by the angle,  $\phi$ , with respect to the  $x$  (sliding) axis. The calculation was carried out using the mean experimental value of the coefficient of friction, i.e.  $\mu = 0.3$ , and the stress values have been normalized with respect to the maximum Hertzian pressure,  $p_0$ . In addition, the orientation of the principal surface stresses has also been plotted in the Figure. It turns out that the maximum principal stress,  $\sigma_1$ , is only slowly decreasing when the angle,  $\phi$ , is increased from  $0^\circ$  to  $45^\circ$ , i.e. within the range where cracks were experimentally observed. Moreover, the  $\sigma_2/\sigma_1$  ratio remains low within this domain, which indicates that cracks remain nucleated under

a predominantly tensile stress field whatever their location along the contact edge. Interestingly, this contact mechanics analysis also shows that the angle,  $\alpha$ , of the maximum principal stress,  $\sigma_1$ , with respect to the sliding direction is progressively decreased when  $\phi$  is increased, which also corresponds to the experimental observations of cracks orientation (see Fig. 4).

### 3.2. Analysis of the fragmentation patterns

Whatever the considered  $a/h$  ratio, damage processes under (visco)elastic conditions were clearly related to the generation of a network of tensile cracks at the leading edge of the contact. The regular spacing of the observed crack patterns suggests that the cracks are successively nucleated according to an unloading/reloading process within the PS coating. When a crack is nucleated at the leading edge of the contact, it can be assumed that coating stresses are relaxed in its vicinity. Accordingly, the formation of a new crack will require that the tensile stresses are rebuilt within the coating up to some critical value associated with the strength of polystyrene. This film reloading mechanism will occur as a consequence of the relative displacement between the glass slider and the cracks. A critical length can tentatively be attributed to this reloading process, which should be of the order of magnitude of the crack depth. The occurrence of such a fragmentation mechanism is supported by some order of magnitude estimate of the stress intensity factors at the crack tip which can be derived from fracture mechanics solutions for plates with periodic parallel cracks. Analytical calculations derived by Isida [29] indicate that, when the distance,  $b$ , between adjacent cracks become small with respect to their length, the stress intensity factor,  $K_I$ , at the crack tips tends to the following limiting value:  $K_I = \sigma_0 \sqrt{b/\pi}$  where  $\sigma_0$  is the remote tensile stress. The investigated contact configuration is obviously different from a cracked plate configuration in the sense that the PS layer is deposited onto a substrate and that the applied contact stress field is heterogeneous. However, it turns out that, if typical values of  $\sigma_0 = 100$  MPa and  $b = 30$   $\mu\text{m}$  are considered, one gets a value of the critical stress intensity factor,  $K_{IC}$ , of the order of  $0.3 \text{ MPa m}^{1/2}$ , which is the right order of magnitude for the toughness of polystyrene.

The values of the critical lengths associated with the coating's fragmentation mechanisms and their dependence on the film thickness has been considered more in details from a quantitative post mortem analysis of the crack patterns. The mean distance between two adjacent cracks has been measured by image analysis using grey level profiles taken in the middle of the crack pattern and along the sliding direction. As shown in Fig. 6, a mean critical length,  $L_c^{\text{exp}}$ , between cracks can be determined from the statistical distribution of inter-cracks spacing distances. In Fig. 7, experimental data are summarized in a non dimensional plot giving the normalized critical length,  $L_c^{\text{exp}}/h$ , as a function of the ratio  $a/h$ . It appears that all data

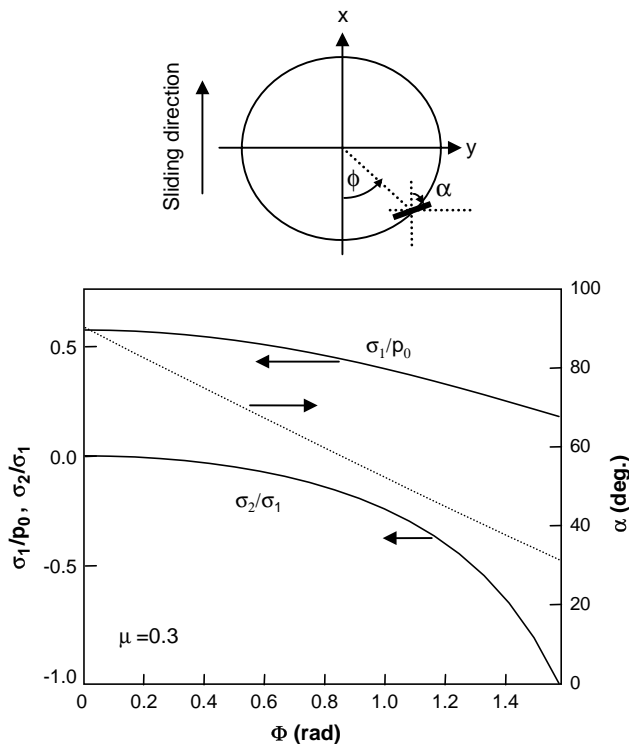


Fig. 5. Calculated values and orientation of the surface principal stresses along the leading edge of the contact. The calculation have been performed using Hamilton's theory [26], a value of the coefficient of friction equal to 0.3 and average values of the elastic constants reported in table I. The maximum principal stress,  $\sigma_1$ , has been normalized with respect to the maximum Hertzian pressure,  $p_0$ . Cracks were observed experimentally for  $0 < \phi < 45^\circ$ . The values of the ratio  $\sigma_2/\sigma_1$  show the essentially tensile nature of the cracks within this range.

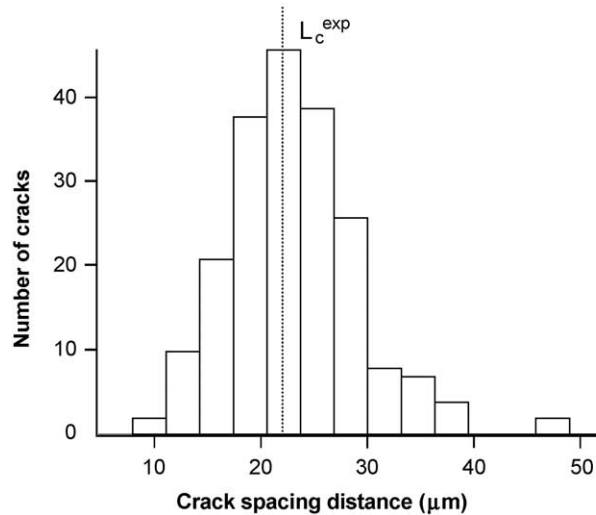
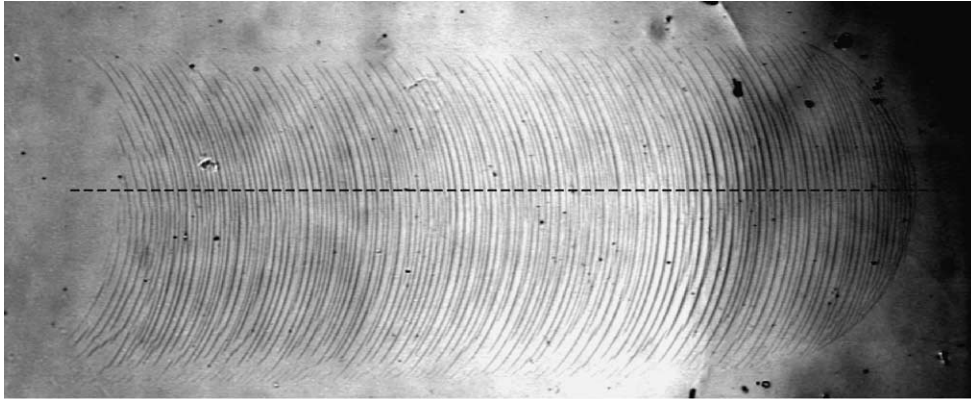


Fig. 6. Determination of the statistical distribution of the distances between two adjacent cracks from post mortem observations of the sliding traces. The mean experimental critical length,  $L_c^{\text{exp}}$ , between adjacent cracks is taken from the maximum in the distribution.

points obtained for  $al/h$  ratios ranging from 1 to 100 rescale on a single scatter band, independently on the film thickness (from 10 to 100  $\mu\text{m}$ ) and with some evidence of a saturation of  $L_c^{\text{exp}}/h$  when  $al/h$  exceeds about 60. The fact that  $L_c^{\text{exp}}/h$  is continuously decreasing below this threshold  $al/h$  ratio can tentatively be interpreted by the fact that the stress gradients associated with the tensile reloading of the film at the vicinity of a crack become steeper for small contact radii. As a result, the tensile reloading of the film up to failure should occur over a decreased length with respect to the crack depth, i.e. with respect to the film thickness if cracks are assumed to propagate up to the interface.

It is also worth noting that, depending on the contact loading conditions (contact radius, applied normal force), different frictional forces and contact stresses were achieved, but that these parameters did not affect significantly the normalized critical length for a given  $al/h$  ratio. From frictional force measurements under elastic conditions, the maximum tensile stresses at the edge of the contact were found, using Hamilton's approach, to range from about 40 to 100 MPa, i.e. values greater than the threshold tensile stress for craze nucleation in polystyrene

(20–30 MPa) [30]. This result tends to show that, provided the contact stresses are greater than the coating failure stress, the fragmentation pattern is relatively independent on the magnitude of the tangential loading.

#### 4. Contact mechanics analysis of the fragmentation processes

The above detailed cracking mechanisms present close similarities with the fragmentation processes which are observed in many heterogeneous systems such as fibre reinforced composites [31,32] paints or coatings [33,34], where a brittle phase is intimately associated with a more ductile phase and loaded under tensile conditions. Independently on the system geometry, a saturation of the mean distance between adjacent cracks is often observed when the applied strain is increased. The value of this critical length can be shown to be governed by the statistical distribution of the failure properties of the brittle phase and by the stress transfer processes occurring at the interface [34]. Interface shear stress concentrations at

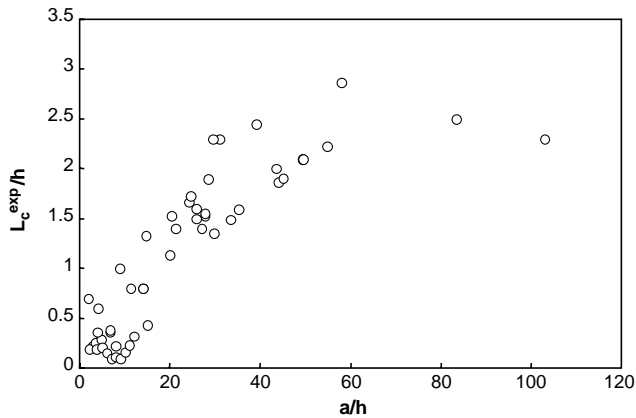


Fig. 7. Experimental values of the normalized critical length,  $L_c^{\text{exp}}/h$ , as a function of the normalized contact radius,  $a/h$ . These values were obtained for film thicknesses ranging from 10 to 100  $\mu\text{m}$  and contact radii varying between 30  $\mu\text{m}$  and 1 mm.

the vicinity of the failure points are often reported to induce some debonding, which in turn increases the critical lengths associated with stress transfer and tensile failure. As a result, interface properties can play a major role in fragmentation processes. Within the context of the present investigation, the sensitivity of the observed fragmentation processes to interface properties have been considered by performing some sliding tests using specimens without the block copolymer layer at the PMMA/PS interface. According, to Brown et al. [13], such a modification can result in a dramatic decrease in the mode I interface fracture energy. However, no significant change in the measured critical fragmentation lengths was observed for the sliding conditions under consideration. Moreover, no evidence of a flaking-off of the PS coating was observed during the sliding tests. In the absence of any detectable interface effect, a perfect bonding between the PS coating and the PMMA substrate was therefore assumed in the subsequent mechanical analysis of fragmentation processes.

In order to assess the changes in the critical length as a function of the film thickness and the contact radius, contact mechanics simulations have been carried out by considering an equivalent bidimensional contact between a cylindrical indenter and an elastic body containing a single crack oriented perpendicular to the surface (Fig. 8). This two-dimensional approach avoided the complexities of three-dimensional numerical simulations of cracked contacts. Moreover, the validity of such a two dimensional approach is supported by the fact that the magnitude of the contact tensile stresses did not vary very significantly in the area where cracks were observed (see principal stress calculations in Section 3.1). Due to the similarity of the PMMA and PS moduli, the cracked substrate was considered as a homogeneous body, where the crack depth corresponds to the coating thickness. As detailed below, the validity of this later assumption was indirectly supported by an estimate of the crack tip stress intensity factors.

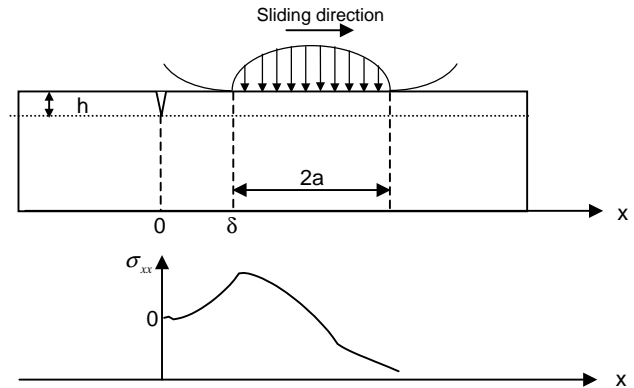


Fig. 8. Schematic description of the two dimensional geometry considered for the numerical contact mechanics simulations of the cracked coatings.  $\delta$  is the distance between the crack and the leading edge of the sliding contact.  $\sigma_{xx}$  is the calculated surface tensile stress. Both the coating and the substrate are assumed to behave elastically and the depth of the crack is set to the coating thickness.

In a first approach, interactions between adjacent cracks were neglected and the simulations have been carried out considering an isolated crack. The simulations have been performed for different  $a/h$  ratios, while keeping constant the maximum value of the Hertzian pressure ( $p_0 = 100$  MPa) and the coefficient of friction ( $\mu = 0.3$ ). During the calculations, the profile of the surface tractions associated with the sliding of the rigid sphere was incrementally shifted from a reference position. As shown in Fig. 8, this reference position was defined as the  $x$  coordinate where the trailing edge of the contact coincides with the crack location.

In a first stage, the values of the mode I stress intensity factors,  $K_I$ , at the crack tip were estimated. As sliding proceeds from the initial indenter position, the crack is opened by the tensile stresses and  $K_I$  is progressively increased up to a maximum value (Fig. 9a). Above this maximum,  $K_I$  decreases as the contact stress field is displaced far from the crack location. The value of the maximum in  $K_I$  has been reported as a function of the contact radius to film thickness ratio in Fig. 9b. Within the experimental  $a/h$  range, the maximum stress intensity factors are close to the toughness of polystyrene, which support the hypothesis of cracks propagating through the whole coating thickness.

The profiles of the surface tensile stress in the vicinity of a crack have also been calculated for different values of the sliding distance normalized with respect to the contact radius. Fig. 10 shows an example of such a simulation for a moderate  $a/h$  ratio equal to 2. The profiles are characterized by the existence of a peak stress whose location corresponds to the leading edge of the contact, similarly to what would be calculated for an uncracked Hertzian contact. However, for the considered sliding distances, the magnitude of the tensile peak stress is much lower than that for an uncracked substrate (i.e.  $\sigma_{xx}^{\text{max}} = 2\mu p_0 = 60$  MPa). This lowered peak

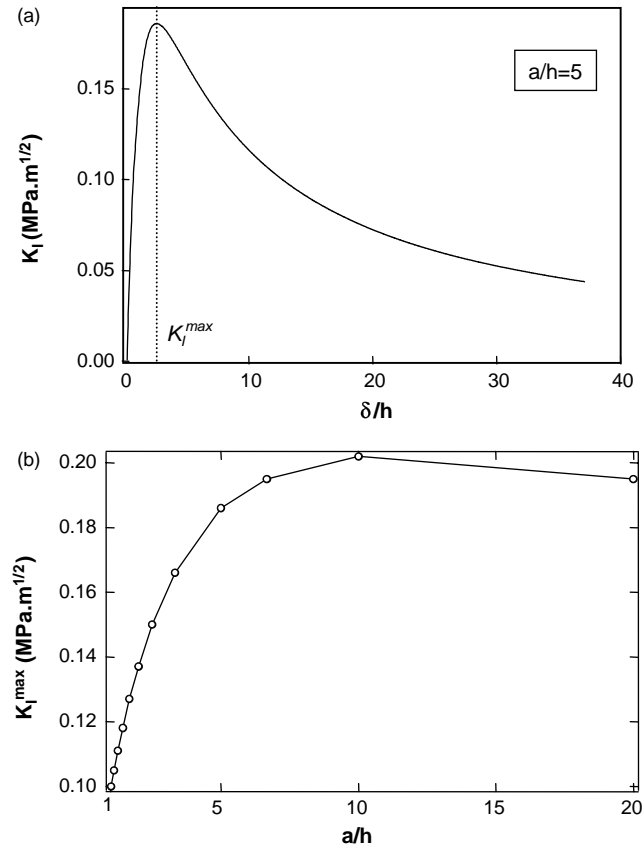


Fig. 9. Calculated values of the mode I stress intensity factor,  $K_I$ , at the tip of a contact crack. The depth of the cracks corresponds to the thickness,  $h$ , of the coating. (a) Changes in  $K_I$  as a function of the sliding distance,  $\delta$ , normalized with respect to the coating thickness. For  $\delta/h=0$ , the leading edge of the contact coincides with crack location. (b) Maximum value of the stress intensity factor,  $K_I^{\max}$ , as a function of the normalized contact radius,  $a/h$ .

stress illustrates the strong relaxation of the coating stresses which results from crack opening processes. When the sliding distance is increased, the tensile reloading of the film is indicated by the progressive increase in the peak stress. Accordingly, a theoretical critical length,  $L_c^{\text{th}}$ , can be defined as the distance relative to the crack location where the calculated peak tensile stress reaches the failure strength of the PS coating. This critical length can be considered as a theoretical prediction of the mean distance between two adjacent cracks. If, for example, a strength of 20 MPa is considered as a failure criterion for the PS layer, the corresponding normalized critical length,  $L_c^{\text{th}}/a$ , can be estimated to be about 0.1.

In Fig. 11, the profiles of surface stresses close to a crack have been reported for a higher  $a/h$  ratio (i.e.  $a/h=100$ ). As opposed to the previous situation ( $a/h=2$ ), the unloading processes associated with the opening of the crack are insufficient to lower the coating stresses below known values of the failure strength of polystyrene. In other words, the simulation indicates that multiple tensile cracks should be nucleated simultaneously close to the leading edge of the contact when the contact radius becomes much

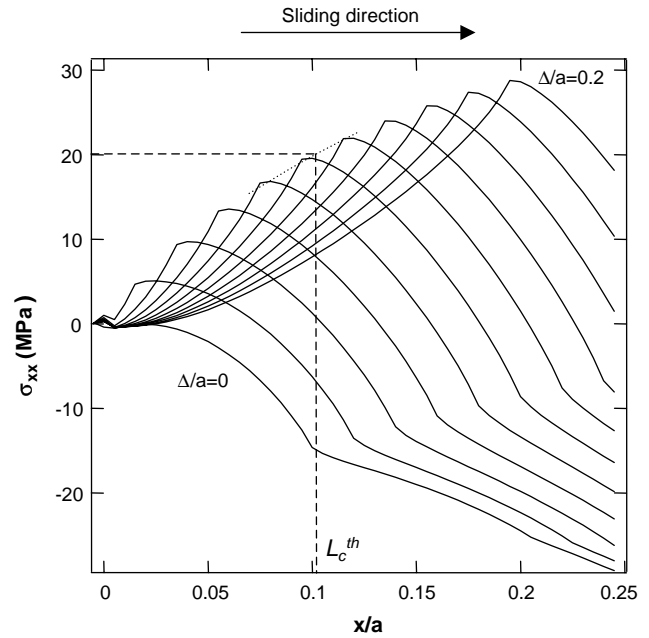


Fig. 10. Calculated surface tensile stress profiles for increasing values of the normalized distance,  $\Delta = \delta/h$ , between the crack and the leading edge of the contact ( $a/h=2$ ). The increment of the normalized displacement between two successive profiles is  $2 \times 10^{-2}$ . The figure shows an example of the determination of the critical reloading length,  $L_c^{\text{th}}$ , assuming that the strength of the coating is 20 MPa.

larger than the coating thickness. This conclusion is consistent with the experimental observations for high  $a/h$  ratios (see Fig. 4) which showed that multiple cracks were indeed simultaneously induced within the contacts. On the other hand, only individual crack nucleation events were observed for contacts with  $a/h$  ratios close to the unity.

In Fig. 12, the theoretical normalized critical lengths,  $L_c^{\text{th}}/h$ , have been reported as a function of  $a/h$  assuming three different values of the coating failure stress, namely 10, 20 and 30 MPa. Whatever the value of this strength criterion, the curves show distinctly a saturation of the critical length at high  $a/h$  ratios. The existence of such a saturation process can be related to the fact that the calculated stress gradient in the vicinity of the crack remains unaffected by its depth above some critical  $a/h$  value. The shaded area in Fig. 12 corresponds to the experimental data band reported in Fig. 7. It can be noted that theoretical data are very consistent with the experimental ones if the failure strength of the film is set to 30 MPa, i.e. a value close to the acknowledged crazing stress of PS. Such a result supports on a quantitative basis the potential assessment of the strength of a polymer coating from fragmentation experiments carried out under sliding conditions.

## 5. Conclusions

The cracking processes of brittle polystyrene coatings on Polymethylmethacrylate substrates have been investigated

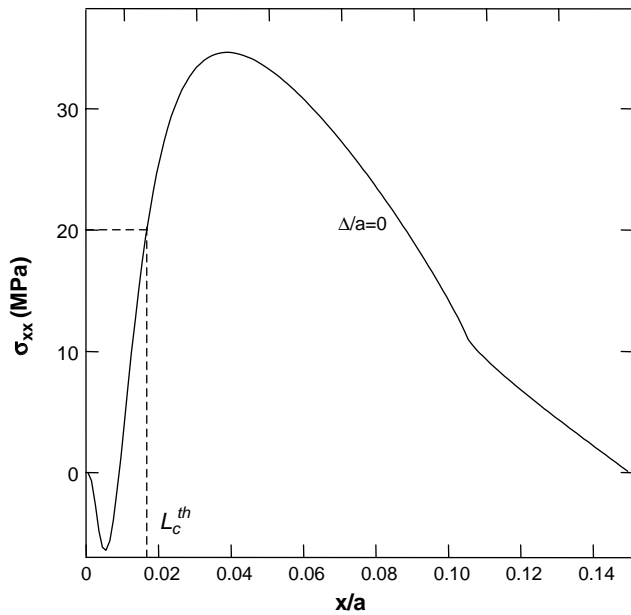


Fig. 11. Calculated surface tensile stress profiles for  $a/h = 100$  and for a null distance between the crack and the leading edge of the contact. The stress relaxation associated with crack opening is insufficient to lower the tensile stress below acknowledged values of the strength of polystyrene (between 20 and 30 MPa). The figure shows an example of the determination of the critical reloading length,  $L_c^{th}$ , assuming that the strength of the coating is 20 MPa.

within sliding contacts with rigid counterfaces under both elastic and viscoplastic contact conditions. For large contact strains (i.e.  $a/R > 0.2$ ), cracks convex to the wake of the indenter were nucleated at the front edge of the contact, in regions where a significant viscoplastic pile-up was observed. Under elastic and viscoelastic contact conditions (i.e.  $a/R < 0.1$ ), the damage of the PS coating was associated with the generation of a network of curved cracks at the leading edge of the contact under the action of

the predominantly tensile stress field. The analysis of these cracking patterns was undertaken within the frame of an analogy with the generic fragmentation processes observed in many brittle coatings under the action of a remote tensile stresses. In such systems, it is generally considered that cracks are induced as a result of stress transfer processes at the coating/substrate interface. For the contact configuration under investigation, the relevant interface for stress transfer was clearly the contact interface as no significant effect of the adhesion between the PS and PMMA layers was observed. As compared to other loading configurations (bending, tension...), one of the main characteristics of the contact loading is that the associated fragmentation processes are not induced under the action of a remote homogenous tensile stress field, but under the action of the moving contact stress field. Within this context, the progressive nucleation and propagation of cracks at the leading edge of the contact can be attributed to the succession of unloading and reloading stages associated with crack opening and sliding processes, respectively. The validity of this analysis was confirmed by contact mechanics simulations of the cracked contacts which allowed quantifying the critical lengths associated with the tensile reloading of the PS films in the vicinity of a crack as a function of film thickness and contact size. The calculated critical lengths were found in excellent agreement with the experimental data obtained for a wide range of film thicknesses. From a material point of view, it emerged from this contact mechanics analysis that the mean spacing between adjacent cracks could be correlated to the strength of the polymer coating, provided that the ratio of the contact radius to the film thickness is known. Contact fragmentation experiments could therefore be envisaged as an alternative to bulk fragmentation tests in situations where, for example, the geometry is incompatible with the application of an homogenous remote tensile field.

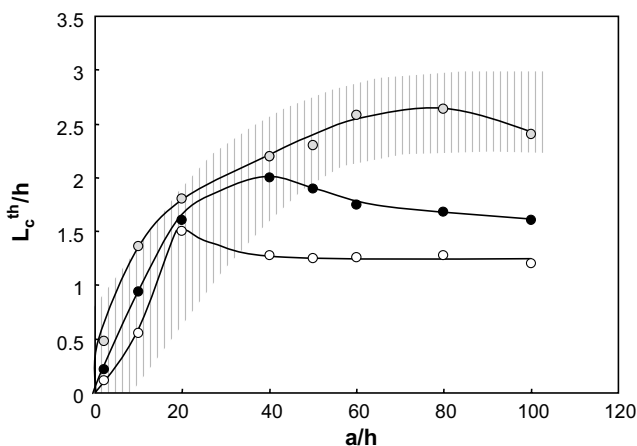


Fig. 12. Theoretical values of the normalized critical length,  $L_c^{th}/h$ , as a function of the normalized contact radius,  $a/h$ . The three curves were obtained assuming different strength failure criteria for the polystyrene layer: (○) 10 MPa, (●) 20 MPa, (○) 30 MPa. The dashed grey area corresponds to the experimental data reported in Fig. 7.

## References

- [1] Briscoe BJ. Isolated contact stress deformations of polymers: the basis for interpreting polymer tribology. *Tribol Int* 1998;31(1-3): 121–6.
- [2] Gauthier C, R. Schirrer. Time and temperature dependence of the scratch properties of poly(methylmethacrylate) surfaces. *Journal of Materials Science* 2000;35(9):2121–30.
- [3] Gauthier C, Lafaye S, Schirrer R. Elastic recovery of a scratch in a polymeric surface: experiments and analysis. *Tribol Int* 2001;34: 469–79.
- [4] Briscoe BJ, Pelillo E, Sinha SK. Characterisation of the scratch deformation mechanisms for poly(methylmethacrylate) using surface optical reflectivity. *Partnership in polymers. Polymer International* 1997;43(4):359–67.
- [5] Bertrand-Lambotte P, et al. Nano-indentation, scratching and atomic force microscopy for evaluating the mar resistance of automotive clearcoats: study of the ductile scratches. *Thin Solid Films* 2001;398-399:306–12.
- [6] Bertrand-Lambotte P, et al. Understanding of automotive clearcoats scratch resistance. *Thin Solid Films* 2002;420-421:281–6.

- [7] Xiang C, et al. Scratch behavior and material property relationship in polymers. *Journal of Polymer Science: Part B: Polymer Physics* 2000; 39:47–59.
- [8] Yang ACM, Wu TW. Abrasive wear and craze breakdown in polystyrene. *Journal of Materials Science* 1993;28:955–62.
- [9] Briscoe BJ, et al. Scratching maps for polymers. *Wear* 1996;200: 137–47.
- [10] Briscoe BJ, Pelillo E, Sinha SK. Scratch hardness and deformation maps for polycarbonate and polyethylene. *Polym Eng Sci* 1996; 36(24):2996–3005.
- [11] Yang ACM, Wu TW. Wear and friction in glassy polymers: microscratch on blends of polystyrene and poly(2,6-dimethyl-1,4-phenylene oxide). *J Polym Sci B: Polym Phys* 1997;35:1295–309.
- [12] Bethune B. The surface cracking of glassy polymers under a sliding spherical indenter. *J Mater Sci* 1976;11:199–205.
- [13] Brown HR, et al. Effects of diblock copolymer on adhesion between immiscible polymers. 1. PS-PMMA copolymer between PS and PMMA. *Macromolecules* 1993;26:4155–63.
- [14] Lamethe JF, et al. Contact fatigue behaviour of glass polymers with improved toughness under fretting wear conditions. *Wear* 2003;(255): 758–65.
- [15] Dubourg MC, Chateauinois A, Villechaise B. In situ analysis and modeling of crack initiation and propagation within model fretting contacts using polymer materials. *Tribol Int* 2003;36:109–19.
- [16] Dubourg MC, Villechaise B. Analysis of multiple fatigue cracks. Part I: theory. *ASME Journal of Tribology* 1992;114:455–61.
- [17] Cominou M. The interface crack. *Journal of Applied Physics* 1977;45: 287–90.
- [18] Bucaille JL, et al., The influence of strain hardening of polymers on the piling-up phenomenon in scratch tests: experiments and numerical modelling. *Wear in press*.
- [19] Sadeghipour K, et al. Modeling of fatigue crack propagation during sliding wear of polymers. *J Eng Mater Technol-Trans Asme* 2003; 125(2):97–106.
- [20] Zhang HQ, Sadeghipour K, Baran G. Numerical study of polymer surface wear caused by sliding contact. *Wear* 1999;224(1):141–52.
- [21] Chateauinois A, Baietto-Dubourg MC. Fracture of glassy polymers within sliding contacts. In: Kausch H-H, editor. *Intrinsic Molecular Mobility and Toughness of Polymers*. Heidelberg: Springer; 2004.
- [22] Chateauinois A, Kharrat M, Krichen A. Analysis of fretting damage in polymers by means of fretting maps. In: Chandrasekaran V, Elliott CB, editors. *Fretting Fatigue: Current Technology and Practices*. ASTM STP 1367. West Conshohocken: American Society for Testing and Materials; 2000. p. 325–66.
- [23] Kharrat M, Krichen K, Chateauinois A. Analysis of the fretting conditions in a contact between an epoxy thermoset and a glass counterface. *Tribol Trans* 1999;42(2):377–84.
- [24] Lawn BR, Wiederhorn SM, Roberts DE. Effect of sliding friction forces on the strength of brittle materials. *J Mater Sci* 1984;19:2561–9.
- [25] Lawn B. Fracture of brittle solids. In: Davis EA, Ward IM, editors. *Cambridge Solid State Science Series*. 2nd ed. Cambridge: Cambridge University Press; 1993.
- [26] Hamilton GM. Explicit equations for the stresses beneath a sliding spherical contact. *Proceedings of the Institution of Mechanical Engineers* 1983;197C:53–9.
- [27] Lafaye S, Gauthier C, Schirrer R. Analysis of the apparent friction of polymeric surfaces. *J Mater Sci in press*.
- [28] Lafaye S, Gauthier C, Schirrer R. A surface flow line model of a scratching tip: apparent and true local friction coefficients. *Tribol Int* 2004;38(2):113–27.
- [29] Isida M. Effect of width and length on stress intensity factors of internally cracked plates under various boundary conditions. *Int J Fract Mech* 1971;7(3):301–16.
- [30] Kausch HH. Polymer fracture. In: *Polymers—properties and application*, vol. 2. Berlin: Springer; 1978.
- [31] Herrera-Franco PJ, Drzal LT. Comparison of methods for the measurement of fibre/matrix adhesion in composites. *Compos Sci Technol* 1992;23(1):2–25.
- [32] Piggott MR. *Load bearing fibre composites*. 2nd ed. London: Kluwer; 2002.
- [33] Kim SR, Nairn JA. Fracture mechanics analysis of coating/substrate systems. Part II: Experiments in bending. *Eng Fract Mech* 2000;65: 595–607.
- [34] Leterrier Y, et al. Adhesion of silicon Oxide layers on poly(ethylene terephthalate). I: effect of substrate properties on coating's fragmentation process. *J Polym Sci B: Polym Phys* 1997;35:1449–61.
- [35] Passade N, Creton C, Gallot Y. Fracture toughness of interfaces between glassy polymers in a trilayer geometry. *Polymer* 2000;41: 9249–63.